The Astrophysical Journal, 645:470–479, 2006 July 1

THREE-DIMENSIONAL MODELS FOR HIGH-VELOCITY FEATURES IN TYPE Ia SUPERNOVAE

Masaomi Tanaka,[1] Paolo A. Mazzali,[1,2,3] Keiichi Maeda,[4] and Ken'ichi Nomoto[1]

Received 2006 January 17; accepted 2006 March 7

ABSTRACT

Spectral synthesis in three-dimensional space for the earliest spectra of Type Ia supernovae (SNe Ia) is presented. In particular, the high-velocity absorption features that are commonly seen at the earliest epochs (∼10 days before maximum light) are investigated by means of a three-dimensional Monte Carlo spectral synthesis code. The increasing number of early spectra available allows statistical study of the geometry of the ejecta. The observed diversity in strength of the high-velocity features (HVFs) can be explained in terms of a "covering factor," which represents the fraction of the photosphere that is concealed by high-velocity material. Various geometric models involving high-velocity material with a clumpy structure or a thick torus can naturally account for the observed statistics of HVFs. HVFs may be formed by a combination of density and abundance enhancements. Such enhancements may be produced in the explosion itself or may be the result of interaction with circumstellar material or an accretion disk. Models with one or two blobs, as well as a thin torus or disklike enhancement, are unlikely as a standard situation.

Subject headings: radiative transfer — supernovae: general

Online material: color figures

1. INTRODUCTION

Type Ia supernovae (SNe Ia) have found use in cosmology after it was established that the maximum luminosity can be calibrated via an empirical relation between it and the shape of the light curve (LC; Phillips 1993; Riess et al. 1996). The origin of this empirical relation is, however, not fully understood (e.g., Mazzali et al. 2001), mainly because of uncertainties regarding the properties of the explosion mechanism.

A one-parameter ordering scheme similar to the one found for the LC was also proposed for the spectra (Nugent et al. 1995). In this scheme temperature is the driving parameter characterizing the spectra. While this relation may apply near maximum, detailed observations of SNe Ia with extended early-time spectral coverage indicate that SNe Ia with similar LCs may have different absorption-line velocities. In particular, the absorptions of Si II λ6355, S II λ5640, Ca II H and K, and the Ca II IR triplet have been investigated by several authors (e.g., Patat et al. 1996; Hatano et al. 2000; Kotak et al. 2005; Benetti et al. 2005).

Simultaneously, the number of polarization observations has increased (SN 1996X, Wang et al. 1997; SN 1999by, Howell et al. 2001; SN 2001el, Wang et al. 2003; SN 2004dt, Wang et al. 2004), and it has become possible to infer asphericity by means of spectropolarimetry. These results suggest that some SNe Ia have a somewhat aspherical geometry of the photosphere ($\gtrsim$10% for SN 2001el or ∼20% for SN 1999by, assuming an ellipsoidal geometry). An even larger degree of asphericity is inferred for the distribution of intermediate mass elements (at the level of $\lesssim$25%; see Wang et al. 2003). Multidimensional numerical simulations have also suggested that the explosion is aspherical, mainly owing to the nature of the deflagration flame in three-dimensional numerical simulations (Reinecke et al. 2002; Gamezo et al. 2003; Röpke & Hillebrandt 2005).

Recently, high-velocity features (HVFs) in the Ca II IR triplet have been the subject of interest in SN 1994D (Hatano et al. 1999), SN 1999ee (Mazzali et al. 2005a), SN 2000cx (Thomas et al. 2004), SN 2001el (Wang et al. 2003), SN 2003du (Gerardy et al. 2004), and SN2005cg (Quimby et al. 2006). Here, HVFs are defined as absorptions with velocities much higher than the photospheric component, which has a typical velocity $v \sim$ 15,000 km s^{-1} at ∼1 week before maximum. HVFs are often seen detached from the photospheric component, at velocities of 17,000–29,000 km s^{-1}. The above papers discuss the possible origin of HVFs, including primordial metallicity (Lentz et al. 2000), a property of the explosion, and interaction of the SN ejecta with circumstellar matter (CSM). Whatever their origin, understanding HVFs can cast light on the explosion mechanism.

Mazzali et al. (2005a) tried to fit the HVFs of SN 1999ee using abundance or density enhancements. Their results suggest that it is impossible to reproduce HVFs by abundance enhancement only, and ∼0.1 $M_\odot$ of additional material is required if only the density enhancement is assumed. Gerardy et al. (2004) and Quimby et al. (2006) discussed how HVFs may result from interaction with CSM. They obtained good agreement for several features including Mg II and found that 2×10^{-2} and $(5\text{–}7) \times 10^{-3}$ $M_\odot$ of CSM are needed for SN 2003du and SN 2005cg, respectively. It should be noted that the explosion model (i.e., abundance distribution and the density structure) and the way to introduce additional material are not identical with each other. Recently, Mazzali et al. (2005b) have shown that almost all SNe Ia have Ca II IR triplet HVFs at the earliest epochs. These HVFs have velocities ranging from 17,000 to 29,000 km s^{-1} in different supernovae. The ubiquity of HVFs may indicate that they do not come from an extreme environment. Probably, a combination of different phenomena results in the observed HVFs.

The geometry of the ejecta has been studied in multidimensional space. Kasen et al. (2003) analyzed both spectroscopy and spectropolarimetry of SN 2001el and showed that both an aspherical photosphere and a single high-velocity blob can reproduce the observations. Thomas et al. (2004) derived a similar geometry for the Ca II HVFs of SN 2000cx.

[1] Department of Astronomy, Graduate School of Science, University of Tokyo, Hongo 7-3-1, Bunkyo-ku, Tokyo 113-0033, Japan; mtanaka@astron.s.u-tokyo.ac.jp, nomoto@astron.s.u-tokyo.ac.jp.

[2] Max-Planck-Institute für Astrophysik, Karl-Schwarzschild-Strasse 1, D-85741 Garching bei München, Germany; mazzali@mpa-garching.mpg.de.

[3] National Institute for Astrophysics–OATs, Via Tiepolo 11, I-34131 Trieste, Italy.

[4] Department of Earth Science and Astronomy, Graduate School of Arts and Science, University of Tokyo, Meguro-ku, Tokyo 153-8902, Japan; maeda@esa.c.u-tokyo.ac.jp.

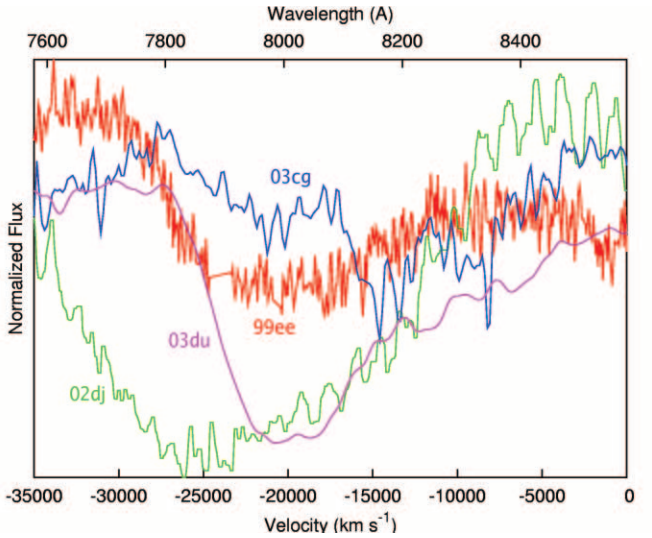

FIG. 1.—Line profiles of the Ca II IR triplet in the early spectra of four SNe. Shown are SN 1999ee (9 days before maximum; Hamuy et al. 2002, *red*), SN 2002dj (11 days before maximum; Kotak et al. 2005, *green*), SN 2003cg (8 days before maximum; Elias-Rosa et al. 2006, *blue*), and SN 2003du (11 days before maximum; V. Stanishev et al. 2006, in preparation, *pink*). The flux was adjusted to have the same continuum flux at $\lambda \sim 7500$–8500 Å by multiplying by a constant. While the HVFs in SN 2002dj and SN 2003du are deep, that of SN 1999ee is weak. SN 2003cg has almost no high-velocity absorption.

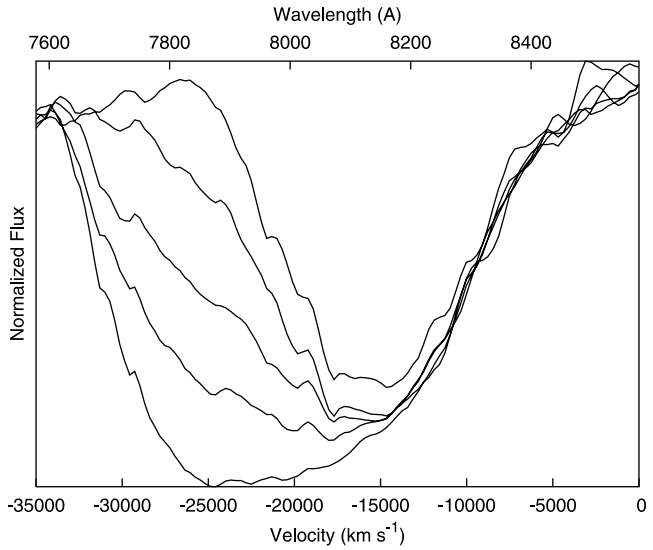

FIG. 2.—Effect of a variation in the strength of high-velocity absorption $S_{\rm HV}$ on the Ca II IR triplet profile. The line optical depth is parameterized as $1-\exp(-\tau)$. The various profiles, going from deeper to shallower absorption, have $1-\exp(-\tau) = 0.9$, 0.7, 0.5, 0.3, and 0.1, respectively, at $v \sim 22{,}000$–$29{,}000$ km s^{-1}. A variation of these parameters does not affect the photospheric absorption at all.

Although all previous studies performed modeling for each SN, no systematic study has been made of the three-dimensional properties of the geometry. We present here synthetic spectra computed in three-dimensional space for various geometries and show how HVFs are affected by different geometric configurations and line-of-sight effects. The increasing number of early spectra available enables us to investigate the statistical properties of HVFs and to constrain the geometry of the ejecta and possibly the nature of the explosion.

In § 2 we discuss how HVFs are formed and suggest a possible parameterized description. In § 3 we present the method of calculation for the spectra and our models. In § 4 the results and some properties of three-dimensional computations are presented. In § 5 the probable geometries that can reproduce the observed trend are discussed. Finally, conclusions including considerations on the origin of the high-velocity material and on the asphericity of the explosion are made in § 6.

2. PROPERTIES OF THE HVFs

HVFs come in different forms. Figure 1 shows the Ca II IR triplet in the earliest spectra of SN 1999ee (9 days before *B* maximum, −9 days), SN 2002dj (−11 days), SN 2003cg (−8 days), and SN 2003du (−11 days). At that epoch, the photospheric velocity is $v_{\rm ph} \sim 12{,}000$–$14{,}000$ km s^{-1}. The photospheric component of the Ca II IR triplet has $v \sim 14{,}000$–$16{,}000$ km s^{-1} in all SNe Ia, as suggested by the data of Mazzali et al. (2005b). This is slightly higher than the photospheric velocity, since the Ca II IR triplet is stronger than Si II or S II and forms above the photosphere. However, the velocities of the absorption minima in SN 1999ee ($\sim$20,000 km s^{-1}), SN 2002dj ($\sim$25,000 km s^{-1}), and SN 2003du ($\sim$20,000 km s^{-1}) are much higher, suggesting that these lines form well above the photosphere. Therefore, the HVFs are expected to have a different origin than the photospheric absorption. Comparing SN 2002dj and SN 2003du, which were observed at the same epoch, it can be noticed that their HVFs have different strength and velocity ranges. The same is true for SN 1999ee and SN 2003du, although their spectra were not taken at exactly the same epoch. At very early epochs, even a small difference in epoch can strongly affect the strength of the photospheric component. However, judging from a number of early spectra, we can safely conclude that there are real variations in the strength of the HVFs. Therefore, we examine a parameterization of the properties of the HVFs based on their velocity range ($v_{\rm HV}$), their strength ($S_{\rm HV}$), and the strength of the photospheric component ($S_{\rm ph}$).

We performed numerical tests to verify what governs the properties of the HVFs. The Monte Carlo SN spectrum synthesis code described in Mazzali & Lucy (1993), Lucy (1999), and Mazzali (2000) was used. The code computes a synthetic spectrum based on the luminosity, the position of the photosphere, the time since the explosion, the density structure, and the abundance distribution. The density structure of the standard deflagration model W7 (Nomoto et al. 1984) was used in all the calculations presented in this section. Photospheric velocity ($v_{\rm ph} = 12{,}500$ km s^{-1}), epoch (8 days since the explosion assuming a rise time of 19 days), and luminosity ($L = 3.0 \times 10^{42}$ ergs s^{-1}) were fixed for simplicity.

First, we consider the case in which $S_{\rm ph}$ and $v_{\rm HV}$ are fixed and parameterize $S_{\rm HV}$ through the line optical depth of the Ca II IR triplet. We assume that the high-velocity region lies at $v_{\rm HV} \sim 22{,}000$–$29{,}000$ km s^{-1}. In this region, the line optical depth is imposed irrespective of the value computed consistently with the W7 structure in order to simplify the investigation of the behavior of HVFs. For example, if the line optical depth is taken as $1-\exp(-\tau) = 0.5$, about half the photons that come into resonance with the Ca II IR triplet are scattered. Figure 2 shows HVFs with various line optical depths $1-\exp(-\tau) = 0.1$–0.9. With this approximation the depth of the HVFs depends almost linearly on $1-\exp(-\tau)$. The origin of the observed diversity in strength is investigated in three-dimensional space in §§ 3 and 4.

Next, we show how the strength of the photospheric component affects the absorption feature. Here $S_{\rm ph}$ is parameterized through the abundance of Ca. In the calculation, a homogeneous abundance distribution is used, which is a reasonable assumption because the region used in the computation is only $v \gtrsim 12{,}500$ km s^{-1}. Figure 3 shows the Ca II IR triplet with

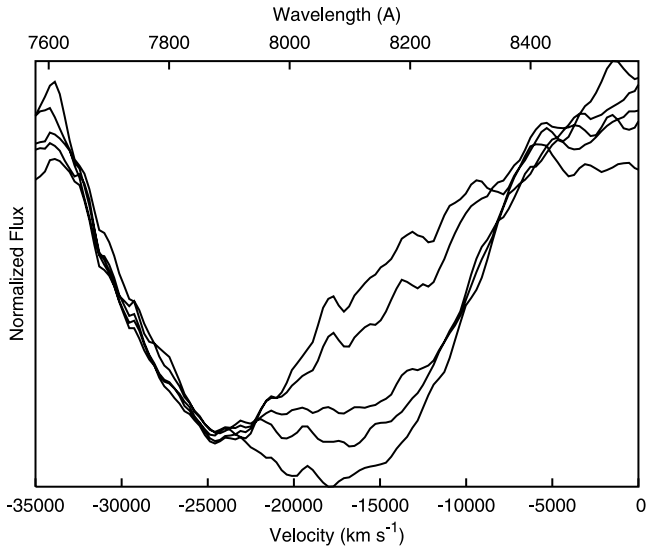

FIG. 3.—Effect of a variation in the strength of photospheric absorption $S_{\rm ph}$ on the Ca II IR triplet profile. The strength is changed through the abundance of Ca. The various profiles, going from deeper to shallower, correspond to a mass fraction $X(\mathrm{Ca}) = 0.068$, 0.034, 0.017, 0.008, and 0.004, respectively. The high-velocity absorption is not affected at all, because we fix the value of $1 - \exp(-\tau) = 0.7$ and the velocity separation between the photospheric component and the HVF is too large.

various strengths of the photospheric component. The mass fraction of Ca is $X(\mathrm{Ca}) = 0.068$, 0.034, 0.017, 0.008, and 0.04. The photospheric absorption depth does not change linearly with the abundance, and the line becomes saturated if the abundance is more than $\sim$1%. Since in this calculation the line optical depth at high velocity is fixed as $1 - \exp(-\tau) = 0.7$ and the velocity separation is large, the HVFs are not affected by the photospheric component.

Using only the abundance of Ca to change the strength of the photospheric component is not completely realistic, because the line strength also depends strongly on temperature and ionization state. Ca is mostly Ca III at the typical temperature of SNe Ia before maximum ($T \sim 12{,}000$ K), and only a small fraction is Ca II and Ca IV. The strength of the Ca II IR triplet is proportional to temperature because of the behavior of the ionization. We tested models with different luminosities, which yield different temperature structures. We found that even with the highest Ca abundance [$X(\mathrm{Ca}) = 0.068$], when the luminosity is increased by a factor of $\sim$4, the strength of the Ca II IR triplet becomes weaker than in the original model with the lowest Ca abundance, $X(\mathrm{Ca}) = 0.002$. An inverse correlation between the strength of the photospheric component and the luminosity at these early epochs might therefore be expected. To verify this, more observations are needed, and it is necessary to fit these individually to determine the exact photospheric velocity and temperature. This is beyond the scope of this work and will be the subject of a separate investigation (M. Tanaka et al. 2006, in preparation).

The results of the tests we performed by changing $S_{\rm HV}$ and $S_{\rm ph}$ (Figs. 2 and 3) show clearly that changing these two parameters is not enough to reproduce all the observed HVFs. As seen between SN 2002dj and SN 2003du in Figure 1 (and see Fig. 4 in Quimby et al. 2006), the widths of the high-velocity absorption are not identical among SNe that have similar depths of the HVFs. No combination of $S_{\rm HV}$ and $S_{\rm ph}$, however, can account for such a difference. Therefore, we conclude that the additional parameter $v_{\rm HV}$ is also needed. One might think that this is because of our assumption of spherical symmetry. However, we obtain the same results in three-dimensional geometry (§ 4). Figure 4 shows how the three parameters ($S_{\rm HV}$, $v_{\rm HV}$, and $S_{\rm ph}$) work. Their combination determines the depth and shape of the absorption and the position of the absorption minimum. Although the luminosity and the photospheric velocity are not fine-tuned, the shape of the absorption feature is reproduced well.

The numerical tests presented here may be somewhat unrealistic, because we assumed a detached spherical shell that is optically thick to the Ca II line, and it is probably more realistic to consider three-dimensional structures. The explosion may be aspherical and have fragmentations (yielding a clumpy structure), or interaction between the SN ejecta and a circumstellar disk may occur (yielding a torus-like structure). In § 3 we use three-dimensional models to see what the three parameters used in this section (i.e., $S_{\rm HV}$, $v_{\rm HV}$, and $S_{\rm ph}$) physically mean.

3. METHOD AND MODELS IN THREE-DIMENSIONAL SPACE

3.1. *Three-dimensional Monte Carlo Code*

To investigate three-dimensional effects on the HVFs, synthetic spectra are calculated assuming various geometries (§ 3.2). We have developed a three-dimensional Monte Carlo radiative transfer code based on the one-dimensional Monte Carlo code described in Mazzali & Lucy (1993), Lucy (1999), and Mazzali (2000). The code assumes the Sobolev approximation and a sharply defined photosphere above which there is no energy deposition. Spherical coordinates are used in the code in order to treat the photosphere precisely. The number of meshes depends on the model and is typically $20 \times 20 \times 20$ for r, $\cos(\theta)$, and ϕ, respectively. The path of the energy packets is traced in three-dimensional space, and the effect of backscattering into the photosphere is included. The line treatment is free from the approximation of resonance scattering; i.e., photon branching is considered correctly as outlined by Lucy (1999). The free parameters are the luminosity $L(\theta, \phi)$, the photospheric velocity $v_{\rm ph}(\theta, \phi)$, and the epoch since the explosion t, all of which are defined as in the one-dimensional code. Although angle-dependent L and $v_{\rm ph}$ can be used in the code, here we assume them to be uniform for simplicity. We again assume $v_{\rm ph} = 12{,}500$ km s^{-1}, $t = 8.0$ days since the explosion, and $L = 3.0 \times 10^{42}$ ergs s^{-1} as typical values for the earliest spectra of SNe Ia. With these parameters, the temperature structure, excitation, and ionization are computed in all zones using a modified nebular approximation (Mazzali & Lucy 1993). This assumes that there is no net exchange of energy between matter and radiation. Photon flux is collected by recording energy packets at the outer boundaries of the ejecta and is binned into a 50×50 solid angle mesh. Since the path of each packet is affected by the density and temperature structure, the emergent spectrum depends on the orientation.

3.2. *Models*

Our models are based on the spherical deflagration model W7 (Nomoto et al. 1984). We introduced additional material in the outer layers of the ejecta to produce HVFs. We are not concerned here with the origin of this material, which may come from fluctuations of the explosion or from interaction with CSM or an accretion disk. Abundance enhancements are not considered, because they have been shown not to be suitable for reproducing HVFs (Mazzali et al. 2005a). The velocity range and the degree of density enhancement are determined by fitting one of the strongest Ca II HVFs, that of SN 2002dj, with the one-dimensional code. As a result, $\sim$0.1 $M_\odot$ of material at $v \sim 22{,}000$–$29{,}000$ km s^{-1} is added in a shell.

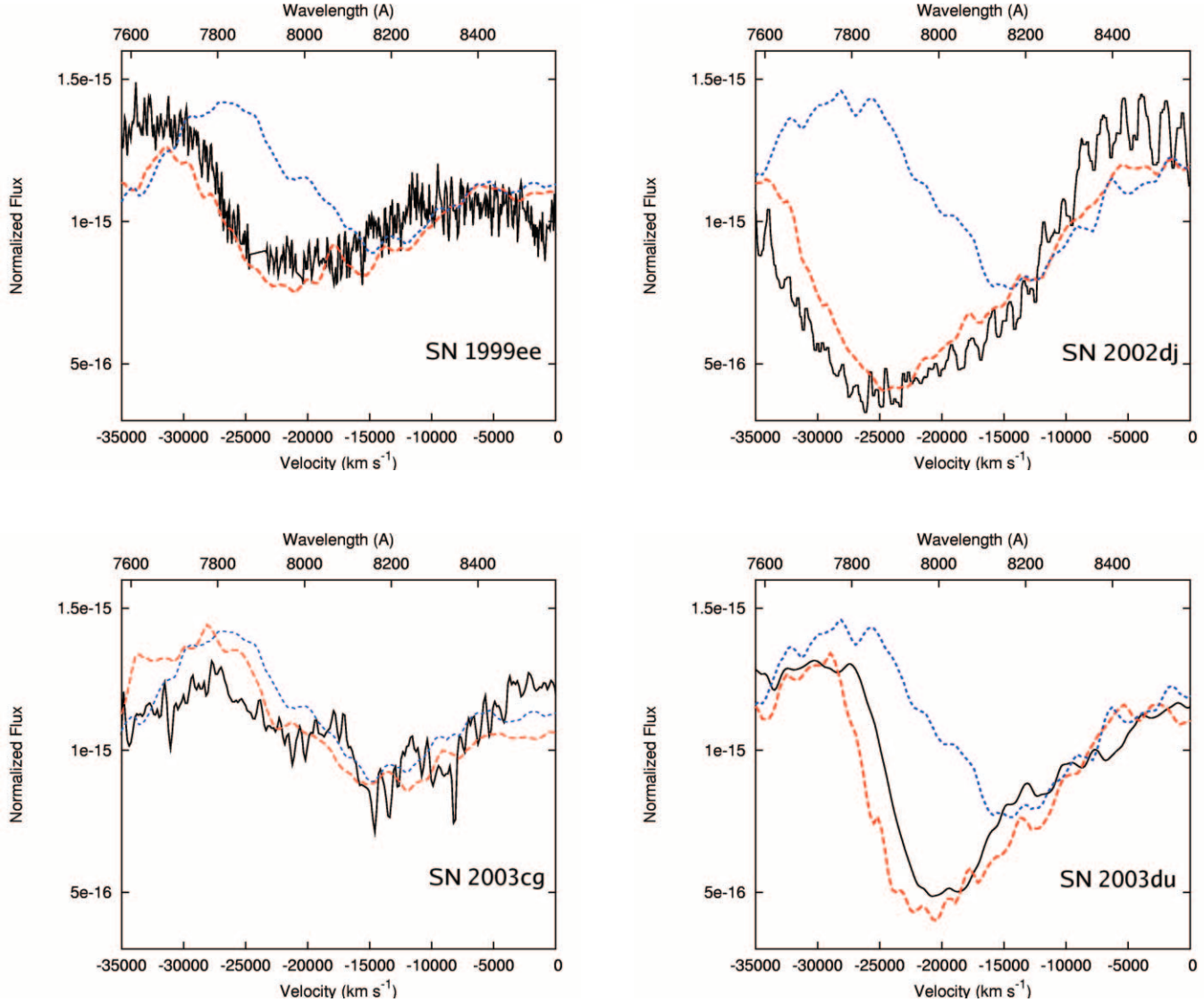

FIG. 4.—Observed Ca II IR triplet (*solid lines*) compared with synthetic spectra computed by adjusting all three parameters ($S_{\rm HV}$, $v_{\rm HV}$, and $S_{\rm ph}$). All spectra are normalized to their continuum level. The red dashed lines are the line profiles computed including the high-velocity components, while the blue dotted lines are the profiles computed with only the photospheric component. Here $S_{\rm HV}$ corresponds to $1 - \exp(-\tau)$, where τ is the line optical depth of the Ca II IR triplet in the high-velocity region and $S_{\rm ph}$ is varied through the abundance of Ca [X(Ca)]. SN 1999ee (9 days before maximum, −9 days; *top left*) is reproduced with $1 - \exp(-\tau) = 0.5$, $v_{\rm HV} \sim 22{,}000$–$27{,}000$ km s^{-1}, and X(Ca) = 0.004. SN 2002dj (−11 days; *top right*) is reproduced with $1 - \exp(-\tau) = 0.7$, $v_{\rm HV} \sim 22{,}000$–$29{,}000$ km s^{-1}, and X(Ca) = 0.008. SN 2003cg (−8 days; *bottom left*) is reproduced with $1 - \exp(-\tau) = 0.2$, $v_{\rm HV} \sim 22{,}000$–$25{,}000$ km s^{-1}, and X(Ca) = 0.004. SN 2003du (−11 days; *bottom right*) is reproduced with $1 - \exp(-\tau) = 0.9$, $v_{\rm HV} \sim 22{,}000$–$25{,}000$ km s^{-1}, and X(Ca) = 0.008.

We fixed this degree of density enhancement in our three-dimensional computations. We used a density enhancement rather than an artificial line strength, which was used in § 3.1, because we want to explore the cause of HVFs. In fact, a spherical density enhancement has the same effect on the Ca II IR triplet profile as the artificial line strength. However, other lines, such as Si II λ6355, are also affected when using a density enhancement. If the observed behavior of both the Ca II IR triplet and Si II λ6355 is reproduced consistently with a density enhancement, we may conclude that HVFs are due to density enhancements. In addition, the mass invoked in HVFs should be reduced in three-dimensional space. In Mazzali et al. (2005a), a large amount of material ($\sim$0.10 $M_\odot$ in the case of density enhancement only) was required to produce HVFs, and this was a serious concern in the hypothesis that HVFs come from either the explosion or CSM interaction. Although Gerardy et al. (2004) and Quimby et al. (2006) found that only $\sim 2 \times 10^{-2}$ and $\sim(5-7) \times 10^{-3}$ $M_\odot$ are enough for the HVFs of SN 2003du and SN 2005cg, respectively, an HVF that has a higher velocity and a deeper absorption has been observed, like SN 2002dj (see Fig. 1). We give an estimate of the amount of material needed in a three-dimensional calculation.

We mapped the density enhancement into three-dimensional space conserving the radial velocity range and the degree of enhancement derived in the one-dimensional calculations. We tested various morphologies that may be realistic, including one or two large blobs, a small number of discrete blobs, a crowded clumpy structure, and tori of various opening angles.

4. RESULTS

First we describe the general behavior of HVFs in three-dimensional models taking a model with a large blob (model B1) as an example. Figure 5 shows the geometry (*left*) and the synthetic line profile (*right*). In the left panel, the red sphere shows

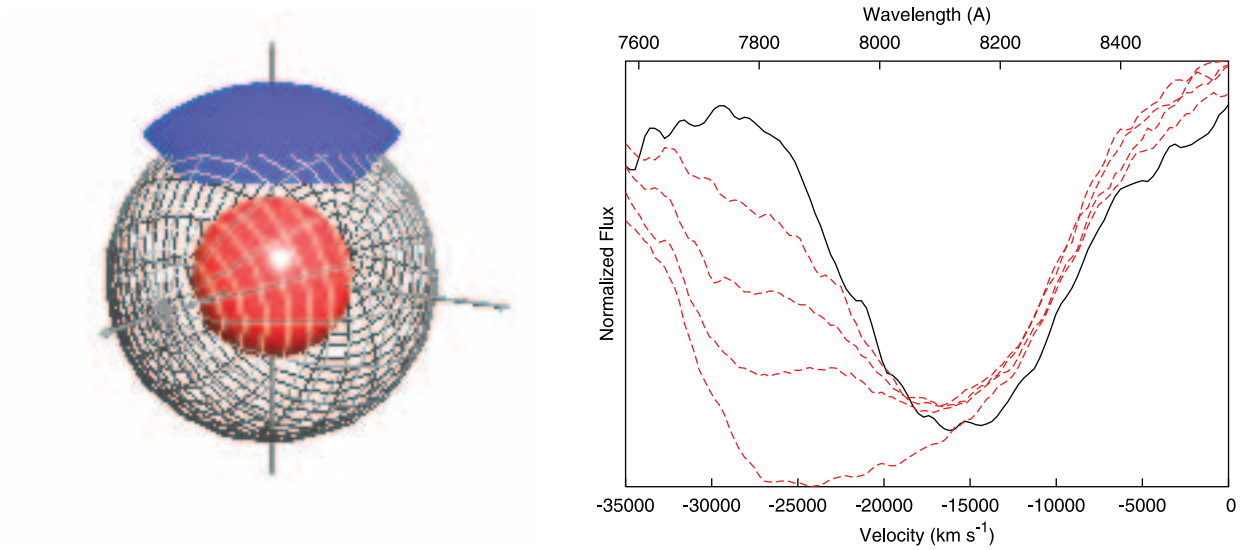

FIG. 5.— Geometry of model B1 (*left*) and synthetic spectra obtained viewing this geometry from different orientations (*right*). The opening angle of the blob is ~80°. The red dashed lines in the right panel show the synthetic spectra corresponding to viewing angles of 0°, 21°, 33°, and 42°, respectively, going from deep to shallow absorption. The angle is measured from the *z*-axis (the direction of the blob). For angles closer to the equatorial plane, the depth of the HVF is almost the same as in the spherical model without any enhancement (*thick line*).

the photosphere and the blue region shows the density enhancement. The depths of HVFs in the synthetic spectra are different for different lines of sight. Seen on the *z*-axis, which is defined as the direction of the blob, the absorption at high velocity is deepest. If we move toward the equatorial plane, the high-velocity absorption becomes shallower and shallower, and it disappears when the line of sight reaches the edge of the blob. Note that having the blob on one side has only a small effect on the emission profile, because the volume occupied by the blob is small. The range of profiles in the right panel of Figure 5 is qualitatively very similar to Figure 2, which shows that our one-dimensional parameterization captures the role of the blobs. If the blob is optically thick, the depth of the HVFs is determined by the fraction of the projected photosphere that is concealed by the dense blob for each line of sight. We define this as the "covering factor" and denote it as *f*.

Figure 6 shows that the HVFs obtained using different covering factors in three-dimensional models resemble those obtained with one-dimensional synthetic spectra for different values of $1 - \exp(-\tau)$. The values are not exactly the same, because our three-dimensional blobs are not infinitely optically thick. In fact, given a typical optical depth τ_0 in the blobs, one expects a relation $\exp(-\tau) \sim (1 - f) + f \exp(-\tau_0)$, where τ is the line optical depth introduced in the one-dimensional computation. Thus, $f = 1 - \exp(-\tau)$ if $\tau_0 = \infty$. Since τ_0 has a finite value, $f \sim [1 - \exp(-\tau)]/[1 - \exp(-\tau_0)]$, which is smaller than the value in an infinitely thick case. Figure 6 clearly indicates this.

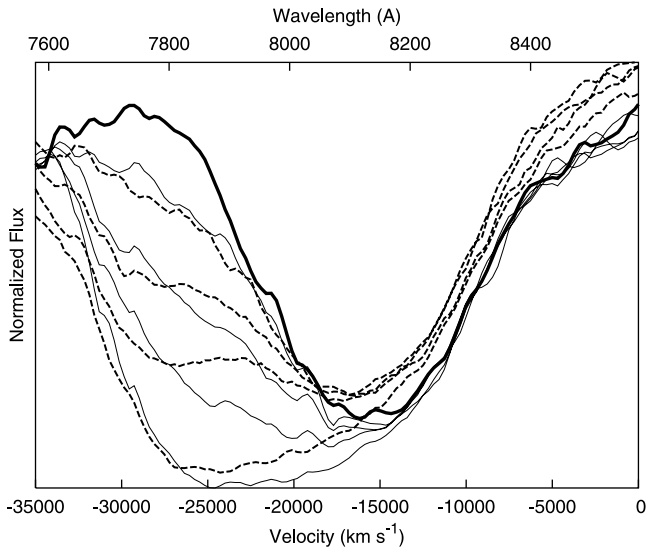

FIG. 6.—Three-dimensional synthetic spectra computed from model B1 (*dashed lines*) compared with the one-dimensional results of Fig. 2 (*solid lines*). While the one-dimensional results have been obtained for shells with different opacities, the three-dimensional spectra correspond to the same model viewed from different angles and therefore differ by the covering factor *f*. The thick line is the model without high-velocity enhancement, or $f = 0$ in three dimensions. The one-dimensional spectra have $1 - \exp(-\tau) = 0.9$, 0.7, 0.5, and 0.3, from deeper to shallower. The three-dimensional spectra have a covering factor $f =$ 1.0, 0.88, 0.66, and 0.46, from deeper to shallower. One- and three-dimensional results are related. The difference between the values of *f* and $1 - \exp(-\tau)$ comes from the fact that the blob in the three-dimensional model is not infinitely thick (see § 4). [*See the electronic edition of the Journal for a color version of this figure.*]

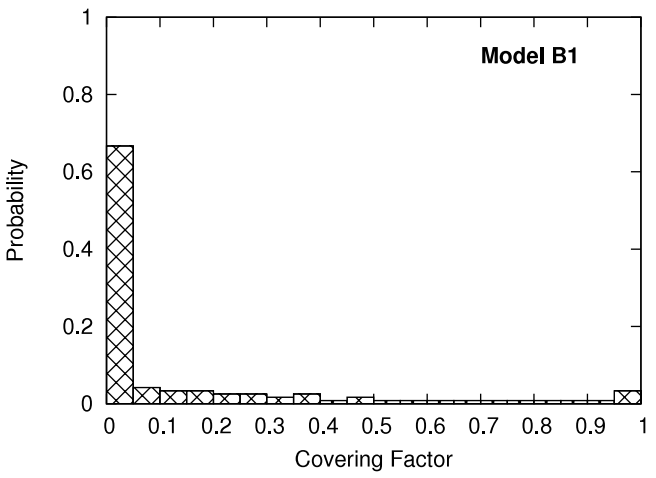

FIG. 7.—Probability distribution of the covering factor *f* in model B1. The horizontal axis shows the covering factor, and the vertical axis shows the frequency of the covering factor if we see this model from various lines of sight.

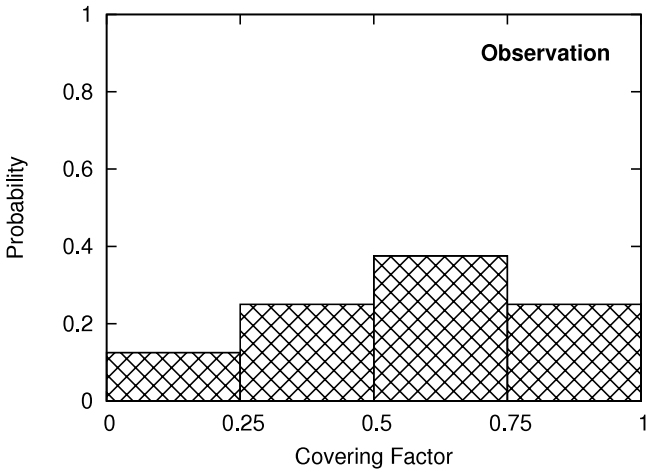

FIG. 8.—Probability distribution of the observed HVFs. Eight SNe from Mazzali et al. (2005a, 2005b) are distributed into four bins by fitting the depths of the HVFs. Note that the number of bins is not identical with the other histogram of the covering factor *f*.

Comparing the values of $1 - \exp(-\tau)$ and f that yield similar spectra shows that the effective τ_0 of the three-dimensional blob decreases with increasing angle. This is probably because the average length of a segment crossing the blob is smaller for larger angles, as there are more grazing trajectories.

If such a blob exists, the variation of the strength of the HVFs ($S_{\rm HV}$) can be reproduced along various lines of sight without introducing unknown parameters such as the line optical depth $1 - \exp(-\tau)$ in § 2. We roughly classify the HVFs by their strength into three groups, strong HVFs ($f \gtrsim 0.7$), medium HVFs ($f \sim 0.45$–0.7), and weak HVFs ($f \lesssim 0.45$). For example, SN 2002dj and SN 2003du have strong HVFs, SN 1999ee has a medium HVF, and SN 2003cg is weak (see Fig. 1).

However, we have to consider the statistical properties of HVFs. Recent observations suggest that a considerable fraction of the earliest spectra have high-velocity absorption. On the other hand, model B1 suggests that a strong HVF will be observed in only ~0.5% of all SNe. Figure 7 is a histogram of the covering factor *f*. It clearly indicates that only a very few orientations can produce strong HVFs, and about 90% of the observations ($f \lesssim 0.45$) should show only the photospheric absorption. Figure 8 shows the observed frequency of the HVFs' strength, made from Mazzali et al. (2005a, 2005b) by distributing eight SNe into four bins. The observed depth of the HVF is converted to the covering factor thorough the numerical fit, as in Figure 4. It should be noted that the number of SNe in the sample is not enough in Figure 8, but the ubiquity of the HVFs is not overthrown even if we consider other SNe (Mazzali et al. 2005b). The clear differences between the histogram of model B1 (Fig. 7) and the observation (Fig. 8) are seen at $f \sim 0.0$ (too much in model B1) and $\gtrsim 0.5$ (too small in model B1). Although it is of course not necessarily required that all observations are reproduced with a single geometry, a general geometry may be inferred if a certain model can reproduce the observed trend. We investigate several geometric models in the following subsections and compare the distribution of synthetic properties to the observed trend.

4.1. *Blob Models*

We showed that a model with one blob is unlikely as a general geometry of SNe Ia. We therefore vary both the size of the blobs and their number. We show the expected statistical properties of each model by means of the distribution of covering factors, since we have shown that there is a direct correspondence between *f* and HVF strength. Figure 9 shows the distribution of covering factors in a model with two blobs (model B2). As expected, the fraction of lines of sight with large covering factors doubles, and the fraction of small factors decreases. This is, however, still not consistent with the fact that most spectra have high-velocity absorption. Although we tested various blob sizes, most lines of sight have $f \lesssim 0.4$ because of the large space between the two blobs. We then increase the number of blobs, adjusting their size so that the photosphere is not completely covered.

Next, we consider a case with several blobs. Figure 10 shows the distribution of covering factors for a model with six blobs with opening angle 60° (*top*; model B6), a model with five blobs of 80° (*middle*; model B5), and a model with several blobs of 30° (*bottom*; model B30). From top to bottom, the space between the blobs becomes smaller. Synthetic spectra show that the correlation between *f* and the depth of the HVF remains even when the blobs are crowded as in model B30. Model B6 still has a large space between the blobs, making the fraction of small *f* large. In addition, this model is very unlikely to produce the deep absorption required to reproduce the objects like SN 2002dj and SN 2003du (see Figs. 1 and 4), which needs $f \sim 1$.

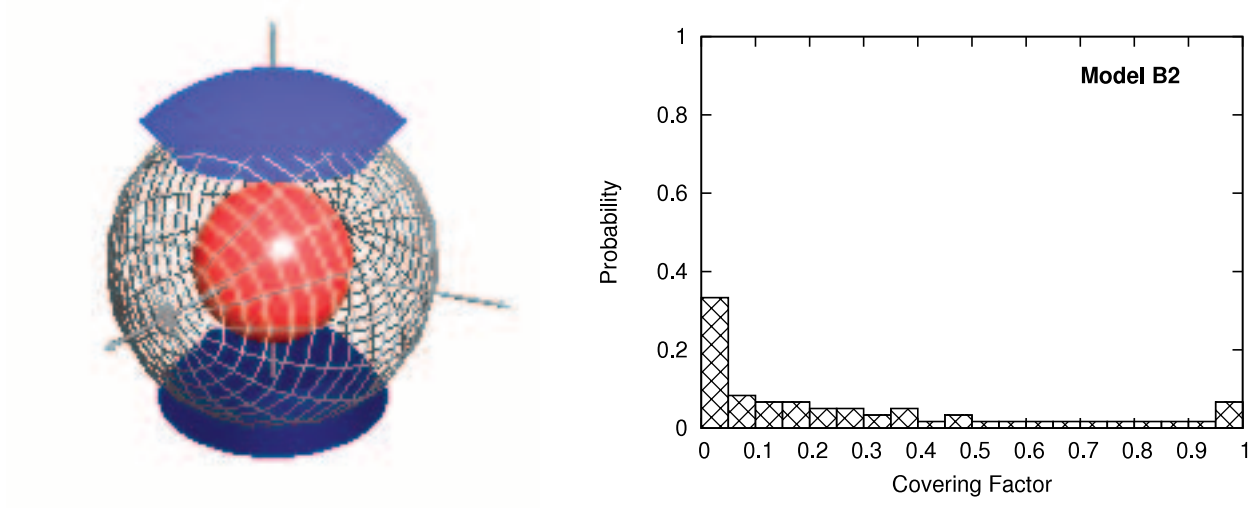

FIG. 9.—Geometry of model B2 (*left*) and distribution of the covering factor (*right*).

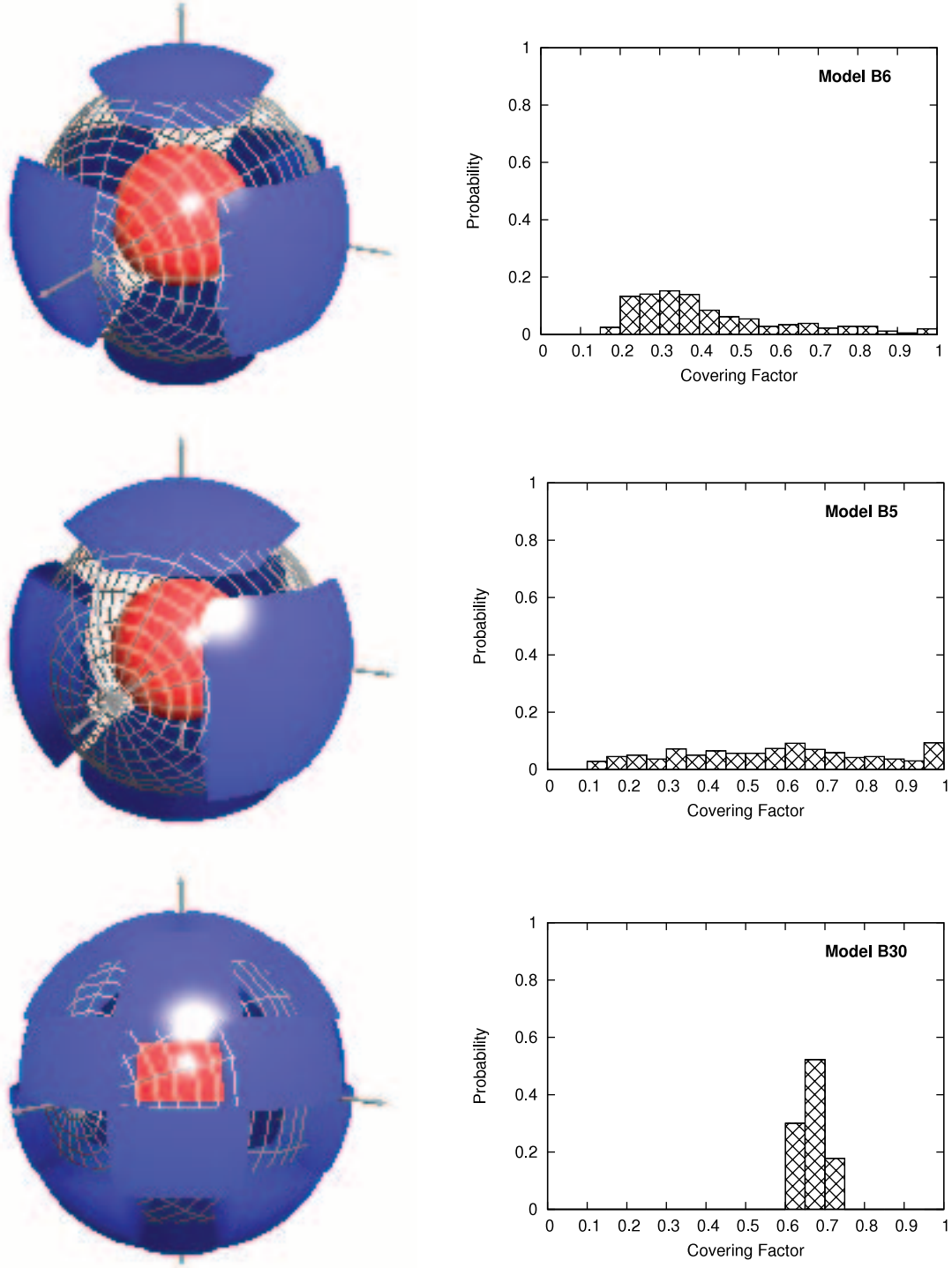

FIG. 10.—*Top:* Geometry of model B6 (six blobs with opening angle 60°) and its distribution of covering factor. *Middle:* Same as the top, but for model B5 (five blobs with opening angle 80°). *Bottom:* Same as the top, but for model B30 (30 blobs with opening angle 30°).

Model B5 (Fig. 10, *middle*) has smaller intervals between the blobs and a large dispersion in the covering factor. This model has a 15% probability of showing a deep absorption ($f \gtrsim 0.9$), while the fraction of lower f is smaller than in any of the models discussed before. The fact that HVFs exist in almost all early spectra may suggest that a clumpy structure like model B5 is a possible average geometry.

If we cram more blobs in (model B30; Fig. 10, *bottom*), the effect of different lines of sight is averaged, and the variation disappears. This result is similar to that of the one-dimensional test with $1 - \exp(-\tau) = 0.5$. Therefore, we can conclude that this geometry is not typical of the majority of SNe Ia, although it may exist.

4.2. *Torus Models*

We distinguish a model that has a torus-like density enhancement from blob models, because the origin of the enhancement is expected to be interaction with CSM or an accretion disk in this case. The main problem with the hypothesis that HVFs come from CSM interaction is the fact that extremely high mass-loss rates are required to place the material just outside the explosion. One expects that this may be solved if the progenitor white dwarf

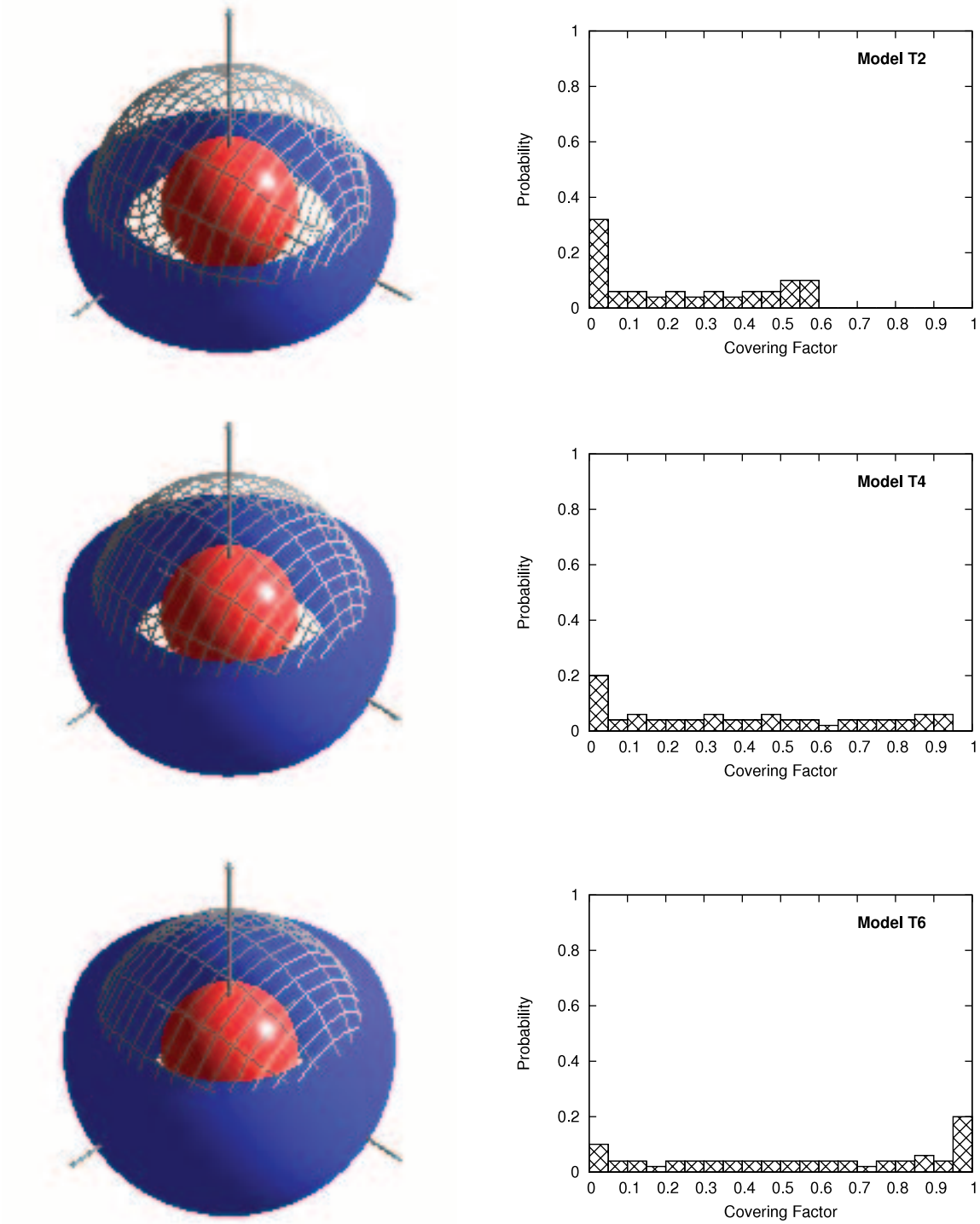

FIG. 11.—Same as Fig. 9, but for torus model T2 (opening angle 20°, *top*), model T4 (opening angle 40°, *middle*), and model T6 (opening angle 60°, *bottom*).

(WD) is surrounded by an accretion disk and the ejecta collide with the disk, leading to density enhancements on the plane of the disk. Figure 11 shows the distribution of covering factors of models with torus-like enhancements (models T2, T4, and T6). These models have a disklike enhanced region with opening angles of 20°, 40°, and 60°, respectively. As shown in the left panels of Figure 11, the 60° disk has a thickness comparable to the diameter of the photosphere.

In model T2 the disk is too thin for the covering factor ever to become large (top panels in Fig. 11). If the thickness increases to 40° (model T4; middle panels in Fig. 11), the fraction of weak HVFs decreases, while those of strong and medium HVFs increase. If the disk is thick enough for the photosphere to be totally concealed, the fraction of strong HVFs increases (model T6; bottom panels in Fig. 11), and the distribution of covering factors becomes broad. Only model T6 may produce the observed distribution of HVF strength.

This implies that a very thick disk is required, with a thickness comparable to the diameter of the WD. The material in the disk should be swept by the SN ejecta in a radial direction, leaving an imprint of the disk's angular size after the explosion. While this may be a realistic model, the absence of hydrogen lines in the

early spectra remains the strongest argument against the disk origin of the HVFs. This problem can be overcome by assuming low temperature ($T \sim 4500$ K) at the shocked ejecta (Gerardy et al. 2004), where the hydrogen lines are less active than metal lines. In addition, see the consideration made in Mazzali et al. (2005a) on the role of hydrogen in making the Ca II IR triplet broad. They estimate $M(\mathrm{H}) \sim 0.004\,M_\odot$ in spherical symmetry.

5. DISCUSSION

The strength of the HVFs (S_{HV}) was parameterized via the line optical depth of the Ca II IR triplet in § 2. The observed range of HVFs can be reproduced using only geometric effects if we assume that the optically thick region is distributed discretely. The covering factor that represents how the photosphere is concealed by the optically thick region acts exactly as $1 - \exp(-\tau)$ in § 2. Among the various geometries discussed in § 4, models B1 and B2 have a very large fraction of lines of sight with $f \lesssim 0.4$, which makes almost no HVFs. Since observations suggest that a considerable fraction of the earliest spectra show HVFs, these models can be ruled out as a standard configuration.

As the interval between the blobs becomes smaller, the fraction of lines of sight with $f \lesssim 0.4$ decreases (e.g., from model B6 to model B30). However, too-crowded structures like model B30 do not give rise to a variation in the covering factor, and so the strength of HVFs is constant. Model B5 has a wide range of covering factors from $f \sim 0.1$ to $f \sim 1$. If such a structure is formed from the explosion, it can explain the observed variety naturally.

It should be noted that models with a hole can be tuned to give the observed distribution of HVFs more easily than models with "blobs" by changing the covering factor, i.e., the size of the hole. How such geometries might be produced is, however, unclear, as they still require a dense high-velocity region and a line of sight that is never far from the hole, because otherwise most SNe would show strong HVFs.

A torus model may reproduce the observed distribution of HVFs if the disk is geometrically thick ($\sim 60^\circ$). Such a thick disklike enhancement could be produced if the accretion disk is thick enough to surround the WD before the explosion. The opening angle of the accretion disk is likely to be reflected in the angular size of a density enhancement.

The torus in model T2 or T4 is so thin that it provides a large fraction of weak features, which are not frequently observed. However, it may be possible to reduce the fraction of $f \lesssim 0.45$ if an interaction with CSM resulting from a spherical or bipolar WD wind occurs. Although many additional parameters should be introduced to investigate the possibility of this scenario, this scenario seems to work qualitatively.

When the optically thick region at high velocity is introduced as a density enhancement, other features are also affected. The Si II λ6355 line is the most notable line, and its behavior has been thoroughly examined (e.g., Benetti et al. 2005). Figure 12 shows spectra around Si II λ6355. If the photosphere is totally covered by dense blobs, the absorption minimum becomes $v \sim 22{,}500$ km s^{-1}. Such high-velocity features have not been observed. In addition, the velocity of Si II λ6355 is not always correlated with that of the Ca II IR triplet in the observed spectra. For example, SN 2002bo has a higher Si II λ6355 velocity ($\sim$15,500 km s^{-1} at -8 days) than that of SN 2003kf ($\sim$12,000 km s^{-1} at -9 days), but the Ca II HVF of SN 2002bo ($v \sim 22{,}000$ km s^{-1}) is slower than that of SN 2003kf ($v \sim 23{,}500$ km s^{-1}). Therefore, the assumption that HVFs in the Ca II IR triplet are due only to density enhancements may not be correct. However, there are some SNe that have an extended blue wing

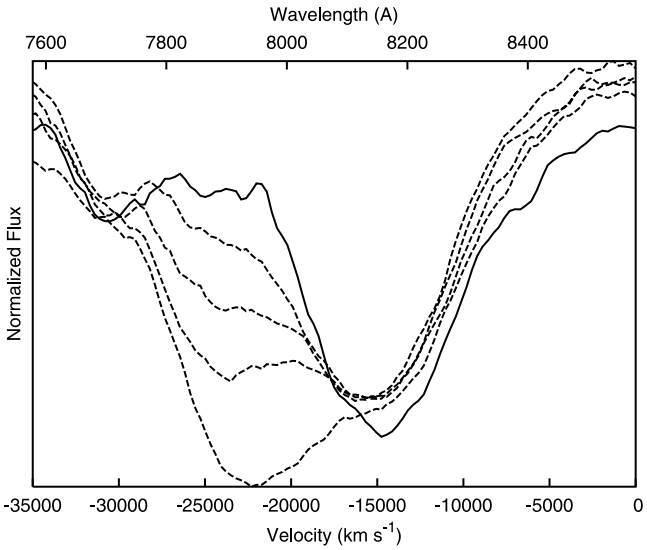

FIG. 12.—Synthetic spectra around Si II λ6355. The thick line is a one-dimensional spectrum without any enhancement. Dashed lines are three-dimensional spectra with covering factor $f = 1.0$, 0.88, 0.66, and 0.46, from deeper to shallower. If the photosphere is totally hidden ($f \sim 1$), the feature forms at a high velocity that has never been observed in any SN. [*See the electronic edition of the Journal for a color version of this figure.*]

in Si II λ6355. This may indicate that some degree of density enhancement also occurs. The combination of density enhancement and abundance enhancement may provide a proper correlation. Such a study, however, is beyond the scope of this work. It is worth noting that the mass of additional material is reduced from $\sim 0.1\,M_\odot$ in the spherical case to $\sim 0.05\,M_\odot$ in models B5, B6, and B30.

The velocity range of HVFs (v_{HV}) is found to be the same in all the models and all the lines of sight as long as the position of the enhancements is fixed. If the covering factor is identical, one might expect that the position of the absorption minimum depends on the line of sight. However, we found that this effect is very slight. The strength of the photospheric absorption S_{ph} is not correlated with the covering factor, and it is not affected even if the line of sight is varied.

6. CONCLUSIONS

We tested the properties of HVFs of the Ca II IR triplet through one-dimensional and three-dimensional modeling. Parameterized one-dimensional simulations were used to extract the main features that determine the HVF. We defined three parameters that govern the HVFs. These are the strength of the HVF S_{HV}, its velocity range v_{HV}, and the strength of the photospheric component S_{ph}. As for S_{HV}, it was shown that geometric effects on models based on high-velocity blobs or a thick torus can provide enough variety to cover all the observations. On the other hand, v_{HV} is not affected by line-of-sight effects. Therefore, we speculate there may be a number of blobs that have different velocities. This might be possible if the WD rotates and the clumpy structure formed by the deflagration flame has different properties depending on direction. Such a variety is not produced in a torus model. However, it may be possible that different disks lead to different enhancements from SN to SN, since the degree of density enhancement and its velocity range depend strongly on the density, the total mass, and the radial extent of the disk.

The strength of the photospheric absorption (S_{ph}) may be influenced by the temperature and the abundance. Although we changed this value by changing the abundance in this paper, it

should be studied whether there is any correlation between the temperature and S_{ph}. This requires knowing the exact temperature and photospheric velocity by fitting observed spectra, which will be the subject of future work (M. Tanaka et al. 2006, in preparation).

The models that best explain the statistics of the observed strength of the HVFs are a blob model (B5) with $\sim$5 blobs of 80° and a thick torus of opening angle $\sim$60°. While a torus model sounds appealing, the main argument against it is the absence of hydrogen lines (but see Gerardy et al. 2004; Mazzali et al. 2005a) and the variation of the HVF velocity. A blob model may result from the explosion if the mushroom structure of the deflagration is not completely washed away in a delayed detonation (Gamezo et al. 2005). Although this does not mean that all the SNe have a single geometry, the average structure may have a distribution of high-velocity material similar to that of model B5. To verify this conclusion, more early-phase observations before maximum are needed. A statistical study can constrain the structure more accurately.

Model B5 is different from the three-dimensional structure that was obtained for SN 2001el by Kasen et al. (2003). Their model has one large blob and an aspherical photosphere and is able to reproduce the observed polarization flux. Our results suggest that such a geometry cannot be standard (see model B1 in § 4). It is completely unknown whether only polarized SNe Ia have such a geometry, consisting of one or two blobs in the outermost region. Rotation of the WD may lead to such a configuration. Although a statistical study of polarization is not available yet, it is potentially useful to verify the geometry, including the abundance distribution. In addition, the statistical study of polarization may be able to distinguish the torus models and the blob models, because the torus-like enhancement tends to produce a large polarization (Kasen et al. 2003).

Detailed hydrodynamic calculations of three-dimensional deflagration flames suffer from a shortage of high-velocity material. It is unknown whether such a result indicates our ignorance about the deflagration flame or the existence of a transition from a deflagration to a detonation. It is therefore quite important to define a suitable explosion mechanism from the observational data. This will be achieved via a statistical study like that presented in this paper when a larger number of early spectra are available. The importance of early observations of SNe Ia cannot be overstated.

This work has been supported in part by the Grant-in-Aid for Scientific Research (16540229, 17030005, 17033002) and the 21st Century COE Program (QUEST) from the JSPS and MEXT (Ministry of Education, Culture, Sports, Science and Technology) of Japan. K. M. is supported through the JSPS (Japan Society for the Promotion of Science) Research Fellowship for Young Scientists.

REFERENCES

Benetti, S., et al. 2005, ApJ, 623, 1011
Elias-Rosa, N., et al. 2006, MNRAS, in press (astro-ph/0603316)
Gamezo, V. N., Khokhlov, A. M., & Oran, E. S. 2005, ApJ, 623, 337
Gamezo, V. N., Khokhlov, A. M., Oran, E. S., Chtchelkanova, A. Y., & Rosenberg, R. O. 2003, Science, 299, 77
Gerardy, C. L., et al. 2004, ApJ, 607, 391
Hamuy, M., et al. 2002, AJ, 124, 417 (erratum 124, 2339)
Hatano, K., Branch, D., Fisher, A., Baron, E., & Filippenko, A. V. 1999, ApJ, 525, 881
Hatano, K., Branch, D., Lentz, E. J., Baron, E., Filippenko, A. V., & Garnavich, P. M. 2000, ApJ, 543, L49
Howell, D. A., Höflich, P., Wang, L., & Wheeler, J. C. 2001, ApJ, 556, 302
Kasen, D., et al. 2003, ApJ, 593, 788
Kotak, R., et al. 2005, A&A, 436, 1021
Lentz, E. J., Baron, E., Branch, D., Hauschildt, P. H., & Nugent, P. E. 2000, ApJ, 530, 966
Lucy, L. B. 1999, A&A, 345, 211
Mazzali, P. A. 2000, A&A, 363, 705
Mazzali, P. A., Benetti, S., Stehle, M., Branch, D., Deng, J., Maeda, K., Nomoto, K., & Hamuy, M. 2005a, MNRAS, 357, 200
Mazzali, P. A., & Lucy, L. B. 1993, A&A, 279, 447
Mazzali, P. A., Nomoto, K., Cappellaro, E., Nakamura, T., Umeda, H., & Iwamoto, K. 2001, ApJ, 547, 988
Mazzali, P. A., et al. 2005b, ApJ, 623, L37
Nomoto, K., Thielemann, F.-K., & Yokoi, K. 1984, ApJ, 286, 644
Nugent, P., Phillips, M., Baron, E., Branch, D., & Hauschildt, P. 1995, ApJ, 455, L147
Patat, F., Benetti, S., Cappellaro, E., Dazinger, I. J., Della Valle, M., Mazzali, P. A., & Turatto, M. 1996, MNRAS, 278, 111
Phillips, M. M. 1993, ApJ, 413, L105
Quimby, R., Hoeflich, P., Kannappan, S. J., Rykoff, E., Rujopakarn, W., Akerlof, C. W., Gerardy, C. L., & Wheeler, J. C. 2006, ApJ, 636, 400
Reinecke, M., Hillebrandt, W., & Niemeyer, J. C. 2002, A&A, 391, 1167
Riess, A. G., Press, W. H., & Kirshner, R. P. 1996, ApJ, 473, 88
Röpke, F. K., & Hillebrandt, W. 2005, A&A, 431, 635
Thomas, R. C., Branch, D., Baron, E., Nomoto, K., Li, W., & Filippenko, A. V. 2004, ApJ, 601, 1019
Wang, L., Baade, D., Höflich, P., Kawabata, K., Khokhlov, A., Nomoto, K., & Patat, F. 2004, ApJ, submitted (astro-ph/0409593)
Wang, L., Wheeler, J. G., & Höflich, P. 1997, ApJ, 476, L27
Wang, L., et al. 2003, ApJ, 591, 1110